

# Measuring the imaginary time dynamics of quantum materials

S. Lederer,<sup>1</sup> D. Jost,<sup>2,3</sup> T. Böhm,<sup>2,3,\*</sup> R. Hackl,<sup>2</sup> E. Berg,<sup>4</sup> and S. A. Kivelson<sup>5</sup>

<sup>1</sup>*Cornell University, Ithaca, New York 14850, USA*

<sup>2</sup>*Walther Meissner Institut, Bayerische Akademie der Wissenschaften, 85748 Garching, Germany*

<sup>3</sup>*Fakultät für Physik E23, Technische Universität München, 85748 Garching, Germany*

<sup>4</sup>*Department of Condensed Matter Physics, The Weizmann Institute of Science, Rehovot, 76100, Israel*

<sup>5</sup>*Department of Physics, Stanford University, Stanford, CA 94305, USA*

(Dated: May 17, 2022)

Theoretical analysis typically involves imaginary-time correlation functions. Inferring real-time dynamical response functions from this information is notoriously difficult. However, as we articulate here, it is straightforward to compute imaginary-time correlators from the *measured* frequency dependence of (real-time) response functions. In addition to facilitating comparison between theory and experiment, the proposed approach can be useful in extracting certain aspects of the (long-time relaxational) dynamics from a complex data set. We illustrate this with an analysis of the nematic response inferred from Raman scattering spectroscopy on the iron-based superconductor  $\text{Ba}(\text{Fe}_{1-x}\text{Co}_x)_2\text{As}_2$ .

Spectroscopic probes provide a wealth of information about the dynamics of quantum systems. Spectra are often very complicated. Sometimes, however, individual spectral features are of less interest than the overall evolution of the spectrum as parameters (such as temperature, pressure, doping, or magnetic field), are varied. In this setting, it is necessary to condense the considerable information in each spectrum into a few numbers. We propose a new method for doing this based on the computation of correlation functions in the *imaginary* time domain. The method is unbiased, numerically reliable, and allows unambiguous comparison with the results of state of the art numerical methods.

It goes without saying that laboratory experiments measure real-time correlators. However, many theoretical methods that have been deployed to extract non-perturbative results on strongly interacting quantum systems, including various forms of quantum Monte Carlo studies, work exclusively in imaginary time. Given the uncertainties in analytic continuation, one reason to compute imaginary time correlators from laboratory data is that it transforms it into a form that can be directly compared with this class of theoretical results.

The transformation from real frequency to imaginary time, discussed in further detail below, discards much of the rich information present in real-time data. For instance, a well defined normal mode (quasiparticle) with an energy  $\epsilon \gg k_B T$  (with  $T$  the temperature) shows up as a sharp peak in an appropriate real frequency response function, but the corresponding feature in the imaginary-time correlator varies as  $\exp[-\epsilon\tau/\hbar]$ , and so makes no contribution to long-time properties. On the other hand, the long time relaxational dynamics of a system—the dynamics that control its approach to equilibrium—typically dominate the long-imaginary time dynamics as well. Thus, using measured response functions to compute long-imaginary-time behavior of the corresponding correlators can be viewed as a method of intrinsic and unbiased filtering, which extracts certain interesting information from a complex spectral response.

In principle, it is possible to compute the real-time (or frequency,  $\omega$ ) fluctuational dynamics of any system in equilibrium from imaginary time (or Matsubara frequency,  $\omega_n$ ) correlation functions and vice versa. In practice, inferring real time dynamics from imaginary time data involves an analytic continuation that can rarely be carried out without additional assumptions. This ambiguity follows from the fact that the discrete Matsubara frequencies,  $\omega_n$ , have spacing  $\Delta\omega \equiv \omega_{n+1} - \omega_n = 2\pi k_B T/\hbar$ , making features which vary as a function of  $\omega$  more rapidly than  $\Delta\omega$  difficult to discern in the imaginary time response functions. It is, however, straightforward to compute imaginary time correlation functions from measured real frequency quantities.

Here, we give explicit formulas for computing imaginary time correlators from response functions measurable in the laboratory. Building on the work in Ref. 1–3, we treat explicitly the general case of linear response of (bosonic) physical observables, as well as the electron spectral function (measurable in tunneling and photoemission spectroscopy). To illustrate what information is emphasized and what is suppressed, we carry out this program for various simple and physically plausible assumed forms of a response function. Finally, we take high resolution Raman data measured on  $\text{Ba}(\text{Fe}_{1-x}\text{Co}_x)_2\text{As}_2$  in the  $B_{2g}$  channel<sup>4</sup> and compute the corresponding imaginary time correlator, which yields a sharp diagnostic of the structural transition in that channel.

## I. COMPUTING IMAGINARY-TIME CORRELATORS FROM SPECTROSCOPIC MEASUREMENTS

### A. Dissipative linear response functions

For any observables  $\Phi_a$  and  $\Phi_b$ , it follows from linear-response theory and the fluctuation dissipation theorem that there is a relation between the dissipative part of the linear response function,  $\chi''_{ab}(\omega)$ , and the imaginary-

time-ordered correlation function,  $\tilde{\Lambda}_{ab}(\tau)$ :

$$\tilde{\Lambda}_{ab}(\tau) = \int \frac{d\omega}{2\pi} \chi''_{ab}(\omega) \left[ \frac{\exp(\omega[\tau - \beta/2])}{\sinh(\beta\omega/2)} \right], \quad (1)$$

where (in units in which  $k_B = \hbar = 1$ )  $\chi''$  is the Fourier transform of

$$\tilde{\chi}''_{ab}(t) \equiv \frac{1}{2} \langle [\Phi_a(t), \Phi_b(0)] \rangle, \quad (2)$$

and, for  $0 \leq \tau \leq \beta$

$$\tilde{\Lambda}_{ab}(\tau) \equiv \langle \Phi_a(-i\tau) \Phi_b(0) \rangle, \quad (3)$$

with  $\beta = 1/T$ . The relation between  $\chi''$  and the imaginary time correlation function in the Matsubara frequency domain is

$$\Lambda_{ab}(\omega_n) = \int \frac{d\omega}{\pi} \chi''_{ab}(\omega) \left[ \frac{\omega}{\omega^2 + \omega_n^2} \right], \quad (4)$$

where  $\omega_n = 2\pi nT$ . Because  $\tilde{\Lambda}_{ab}(\tau)$  is a bosonic correlator,  $\tilde{\Lambda}_{ab}(\tau) = \tilde{\Lambda}_{ab}(\beta - \tau)$ . Thus, if we are interested in the ‘‘long-time’’ behavior of  $\tilde{\Lambda}_{ab}$ , we mean we are interested in the longest-possible times, *i.e.*  $\tau \approx \beta/2$ . The important point to note about Eq. 1 is that for  $\tau \approx \beta/2$ , the integral is dominated by the range of frequencies  $|\omega| \lesssim T$ , so *the long imaginary-time dynamics can be computed from measurements of the response function in a very limited range of frequencies.*

As one important example, let  $\Phi_a$  be a component of the electrical current operator, whose associated susceptibility is proportional to the conductivity. Let  $\sigma'_{aa}(\omega)$  be the real part of the optical conductivity, and  $\tilde{\Lambda}_{aa}(\tau)$  be the imaginary time ordered current-current correlator. Here  $a$  is a tensor index indicating a spatial direction. The Kubo formula relates the conductivity to  $\chi''$ , and consequently<sup>3</sup>

$$\tilde{\Lambda}_{aa}(\tau) = \int \frac{d\omega}{2\pi} \omega \sigma'_{aa}(\omega) \left[ \frac{\cosh[\omega(\beta/2 - \tau)]}{\sinh(\beta\omega/2)} \right]. \quad (5)$$

The other case we treat here is where  $\Phi_a$  is an order parameter field. For instance,  $\Phi_a$  could be a component of the spin density at an appropriate ordering vector  $\vec{Q}$ , so that the resulting susceptibility (which has a singular response near a magnetic transition) can be measured in inelastic neutron scattering. If  $\Phi_a$  is a component of the fermion quadrupole density in some symmetry channel ( $B_{1g}$ ,  $B_{2g}$ , etc.), then the resulting susceptibility (which has a singular response near a nematic transition), can be measured in non-resonant Raman scattering<sup>5</sup>.

## B. Electronic spectral function

Similar expressions relate the imaginary-time-ordered Green function,  $\tilde{G}(\vec{k}, \tau)$  to the single particle spectral

function,  $A(\vec{k}, \omega) \equiv -1/\pi \text{Im}(\mathcal{G}(\vec{k}, \omega))$ , where  $\mathcal{G}$  is the real frequency (retarded) Green function<sup>2</sup>.

$$\begin{aligned} \tilde{G}(\vec{k}, \tau) &= \int d\omega A(\vec{k}, \omega) \left[ \frac{\exp[\omega(\beta/2 - \tau)]}{2 \cosh(\beta\omega/2)} \right], \quad (6) \\ &= \int d\omega I(\vec{k}, \omega) \exp[\omega(\beta - \tau)] \end{aligned}$$

where  $\vec{k}$  is the momentum (or Bloch wave-vector), we have assumed  $\tau$  in the range  $0 \leq \tau < \beta$ , and  $I(\vec{k}, \omega) \equiv f(\omega)A(\vec{k}, \omega)$  is the occupation-weighted spectral function (as measured in ARPES), where  $f(\omega) = [e^{\beta\omega} + 1]^{-1}$  is the Fermi function. Again, except at very short imaginary times, the imaginary time correlator can be readily computed from the experimentally measured response function over a range of frequencies of order  $T$  about the Fermi energy.

In Appendix V we explicitly derive the transformations for a few special cases relevant for correlated systems including the marginal Fermi liquid<sup>6</sup> and power-law scaling close to a quantum critical point.

## II. THE IMAGINARY TIME QUADRAPOLAR CORRELATIONS IN $\text{Ba}(\text{Fe}_{1-x}\text{Co}_x)_2\text{As}_2$

Here we apply the proposed analysis to the measured Raman response of  $\text{Ba}(\text{Fe}_{1-x}\text{Co}_x)_2\text{As}_2$  as a function of  $T$  and doping ( $x$ ), with particular focus on the critical electronic quadrupolar fluctuations in the vicinity of the structural (nematic) transition.

### A. The static susceptibility and $\tilde{\Lambda}(\beta/2)$

Raman scattering measures a dissipative response, and can therefore yield the imaginary part  $\chi''(\omega, T)$  of an appropriate susceptibility. The static value of the susceptibility,  $\chi'(0, T)$ , is often of interest, and is related to  $\chi''(\omega, T)$  by the Kramers-Kronig transformation:

$$\chi'(0, T) = \int \frac{d\omega}{\pi} \frac{\chi''(\omega, T)}{\omega}, \quad (7)$$

Note that Eq. 4 reduces to Eq. 7 when  $\omega_n = 0$ , so that  $\Lambda(0) = \chi'(0, T)$ . In practice,  $\chi'(0, T)$  can almost never be precisely determined from Raman measurements, because the integrand falls off too weakly at large frequency, necessitating an arbitrary cutoff procedure. As an alternative, one can use the same data to determine the value of the imaginary time correlator at time  $\beta/2$ , via

$$\tilde{\Lambda}(\beta/2) = \int \frac{d\omega}{2\pi} \frac{\chi''(\omega)}{\sinh(\beta\omega/2)} \quad (8)$$

Since  $|\sinh(x)| \geq |x|$  for all  $x$  (with the inequality saturated as  $x \rightarrow 0$ ), we have the following inequality:

$$\tilde{\Lambda}(\beta/2) \leq T \int \frac{d\omega}{\pi} \frac{\chi''(\omega)}{\omega} = T\chi'(0), \quad (9)$$

Evidently  $\tilde{\Lambda}(\beta/2)/T$  is bounded above by the static susceptibility, with the bound nearly saturated when spectral weight is concentrated at frequencies  $\omega \ll T$ . In fact,  $\tilde{\Lambda}(\beta/2)/T$  contains the same universal information as the static susceptibility under a wide range of assumptions. For instance, at a continuous phase transition at nonzero temperature,  $\tilde{\Lambda}(\beta/2)/T$  has the same divergent behavior as the static susceptibility. This can be seen by writing the quantity in Fourier transform:

$$\begin{aligned}\tilde{\Lambda}(\beta/2) &= T \sum_n e^{-i\nu_n\beta/2} \Lambda(\nu_n) \\ &= T \sum_n (-1)^n \Lambda(\nu_n) \\ &= T\chi'(0, T) + \dots,\end{aligned}\quad (10)$$

where we have used the fact that  $\Lambda(0) = \chi'(0, T)$ , and dots refer to the contribution from nonzero Matsubara frequencies which, per Eq. 4, are insensitive to the asymptotically low frequencies at which critical behavior in  $\chi''$  is found. At a quantum critical point obeying  $\omega/T$  scaling,  $\tilde{\Lambda}(\beta/2)/T$  also has the same divergence as the static susceptibility in the low temperature limit.

A key practical advantage of  $\tilde{\Lambda}(\beta/2)/T$  as a measure of low frequency fluctuations is the fact that the  $\sinh(\beta\omega/2)$  in the denominator of Eq. 10 yields an exponential cutoff at high energies. This means that  $\tilde{\Lambda}(\beta/2)/T$ , unlike  $\chi'(0)$ , is subject to essentially no error due to a lack of knowledge of high frequencies. As we will show, it is therefore a valuable and unambiguous method of analysis for Raman spectra.

## B. Raman spectra of Co-doped $\text{BaFe}_2\text{As}_2$

We now compare the results for the dimensionless imaginary-time correlation function  $\beta\tilde{\Lambda}(\beta/2, T)$  with the static Raman susceptibility  $\chi'(0, T)$  Fig. 1 shows the analysis of the Raman data of  $\text{Ba}(\text{Fe}_{1-x}\text{Co}_x)_2\text{As}_2$  using Eqs. (8) and (9). At high temperatures the two quantities display a qualitatively similar temperature dependence. As anticipated in Eq. 9  $\beta\tilde{\Lambda}(\beta/2, T)$  is smaller than  $\chi'(0, T)$ .

However, it is important to stress that, for practical purposes, there is an uncertainty in the inferred values of  $\chi'$ . Specifically, since  $\chi''(\omega, T)$  is found to be essentially constant at high energies (see Appendix C), to compute  $\chi'(0, T)$  one must cut off the Kramers-Kronig integral, in which case the result depends logarithmically on the cut-off. In contrast, the weighting factor  $[\sinh(\beta\omega/2)]^{-1}$  in Eq. 8 decays exponentially, making the integral unique so long as the spectra are measured up to energies of a few times the temperature. In any case, as anticipated above,  $\chi'(0, T)$  and  $\beta\tilde{\Lambda}(\beta/2, T)$  have near-identical singularities at the structural transition temperature  $T_s$  in underdoped  $\text{Ba}(\text{Fe}_{1-x}\text{Co}_x)_2\text{As}_2$  with  $x \lesssim 0.06$ . The lack of a genuine divergence at the transition is likely an effect of electron-phonon coupling<sup>8</sup>.

Framing the analysis in terms of  $\beta\tilde{\Lambda}(\beta/2, T)$  has three advantages: (i) It can be computed directly and unam-

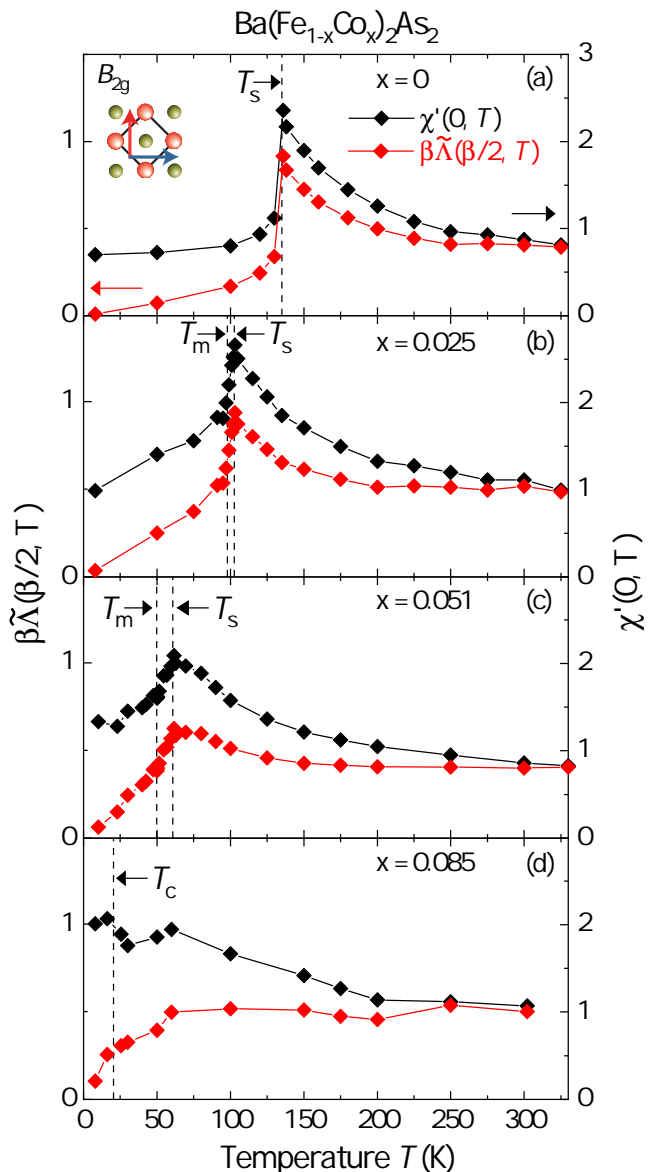


FIG. 1: Temperature dependence of two different measures of the low frequency Raman response of  $\text{Ba}(\text{Fe}_{1-x}\text{Co}_x)_2\text{As}_2$  in the  $B_{2g}$  symmetry channel. Shown in black (right axis) is the static susceptibility  $\chi'(0, T)$ , computed from the measured  $\chi''(\omega, T)$  using the Kramers-Kronig relation of Eq. 7, integrated up to a cutoff frequency of  $1000\text{cm}^{-1}$  (approximately  $123\text{meV}$ ). In red (left axis) is the suitably scaled imaginary time correlation function  $\tilde{\Lambda}(\beta/2, T)$ , defined in Eq. 8. Both quantities capture the singular temperature dependence of the Raman response near the structural transition, but the imaginary time correlator requires no manual cutoff procedure. The two quantities differ most substantially near zero temperature, where  $\tilde{\Lambda}(\beta/2, T)$  must vanish, since it only captures the dynamics at frequencies of order the temperature. The Raman data for  $x \leq 0.051$  are published in Ref. 7, while those with  $x = 0.085$  are shown in Appendix VI.

biguously from the measured  $\chi''$  (ii) the temperature dependence shows a clear dichotomy between underdoped and overdoped materials (compare panels (a), (b), and (c) with panel (d) in Fig. 1), and (iii)  $\beta\tilde{\Lambda}(\beta/2, T)$  can be directly compared with theoretical predictions performed in imaginary time<sup>9</sup>.

### III. DISCUSSION

The advantages of the methods presented here extend to almost any experimental probe which measures response functions at frequencies of order the temperature. In particular, the appropriate response function at maximal imaginary time separation,  $\beta\tilde{\Lambda}(\beta/2)$ , can be computed without an arbitrary cutoff procedure, and is a quantitative measure of low frequency spectral weight. In optical conductivity,  $\beta\tilde{\Lambda}(\beta/2)$  is a physically motivated definition of a low frequency ‘‘Drude weight.’’<sup>10</sup> In inelastic neutron scattering, a drop in  $\beta\tilde{\Lambda}(\beta/2)$  can quantify the development of a spin gap. In angle resolved photoemission spectroscopy, when the signal at high binding energy is sufficiently weak,  $\beta\tilde{\Lambda}(\beta/2)$  is a proxy for the quasiparticle residue  $Z^9$ , and is relatively insensitive to the faint signal at negative binding energy. The experimental measurement of imaginary time response functions is a potentially powerful tool both for the quantification of low frequency spectral properties, and for bridging experiment and theory.

#### Acknowledgments

We acknowledge helpful discussions with A. Baum, M. Randeria, R. Scalettar, and N. Trivedi. D.J. and R.H. gratefully acknowledge the hospitality of the the Stanford Institute for Materials and Energy Sciences (SIMES) at Stanford University and SLAC National Accelerator Laboratory. Financial support for the work came, in part, from the Friedrich-Ebert-Stiftung (D.J.), the Deutsche Forschungsgemeinschaft (DFG) via the Priority Program SPP 1458 (D.J., T.B., and R.H. project no. HA 2071/7-2), the Collaborative Research Center TRR 80 (D.J. and R.H.), and the Bavaria California Technology Center BaCaTeC (S.A.K., D.J., and R.H., project no. 21[2016-2]). SAK was supported in part by NSF grant # DMR-1608055 at Stanford, SL was supported by a Bethe/KIC fellowship at Cornell, and EB was supported by the European Research Council under grant HQMAT (#817799).

### IV. DERIVATION OF EQUATION 1

We begin with the expressions for  $\tilde{\chi}''_{ab}(t)$  and  $\tilde{\Lambda}_{ab}(\tau)$  in Lehmann representation:

$$\tilde{\chi}''_{ab}(t) = \frac{1}{2Z} \sum_{n,m} \Phi_{a,nm} \Phi_{b,mn} [e^{-\beta E_n} - e^{-\beta E_m}] e^{it(E_n - E_m)} \quad (11)$$

$$\tilde{\Lambda}_{ab}(\tau) = \frac{1}{Z} \sum_{n,m} \Phi_{a,nm} \Phi_{b,mn} e^{-\beta E_n} e^{\tau(E_n - E_m)} \quad (12)$$

Fourier transform  $\tilde{\chi}''(t)$  with appropriate regularization at  $t \rightarrow \pm\infty$ , yielding

$$\begin{aligned} \chi''_{ab}(\omega) &= \frac{1}{2Z} \sum_{n,m} \Phi_{a,nm} \Phi_{b,mn} [e^{-\beta E_n} - e^{-\beta E_m}] e^{it(E_n - E_m)} \\ &\quad \times \frac{2 \cdot 0^+}{(\omega + E_n - E_m)^2 + (0^+)^2} \\ &= \frac{1}{2Z} \sum_{n,m} \Phi_{a,nm} \Phi_{b,mn} e^{-\beta E_n} [1 - e^{-\beta\omega}] \\ &\quad \times 2\pi\delta(\omega + E_n - E_m), \end{aligned} \quad (13)$$

with  $0^+$  a positive infinitesimal. We can now write  $\tilde{\Lambda}_{ab}(\tau)$  in terms of  $\chi''_{ab}(\omega)$

$$\begin{aligned} \tilde{\Lambda}_{ab}(\tau) &= \int \frac{d\omega}{\pi} \chi''_{ab}(\omega) \left[ \frac{\exp(-\omega\tau)}{1 - e^{-\beta\omega}} \right] \\ &= \int \frac{d\omega}{2\pi} \chi''_{ab}(\omega) \left[ \frac{\exp[-\omega(\tau - \beta/2)]}{\sinh(\beta\omega/2)} \right], \end{aligned} \quad (14)$$

recovering Eq. 1

### V. EXAMPLE TRANSFORMS

#### A. Nearly constant $\sigma$

The optical conductivity  $\sigma'(\omega)$  is generically an analytic function of  $\omega$ , in which case there is a formal way to compute  $\tilde{\Lambda}$  as

$$\tilde{\Lambda}(\tau) = \pi T^2 \sigma'(\partial_\tau) \sec^2[\pi T(\tau - \beta/2)] \quad (15)$$

If  $\sigma'(\omega)$  varies slowly as a function of  $\omega$  on the scale of  $T$ , then a low order Taylor expansion in  $\omega$  is adequate. Then

$$\begin{aligned} \Lambda(\tau) &= \pi T^2 \sigma'(0) \sec^2[\pi T(\tau - \beta/2)] \times \left\{ 1 \right. \\ &\quad \left. + \alpha_2 \sec^2[\pi T(\tau - \beta/2)] [4 - 2 \cos[2\pi T(\tau - \beta/2)]] \right. \\ &\quad \left. + \dots \right\} \end{aligned} \quad (16)$$

where

$$\alpha_2 = (\pi T)^2 \left[ \frac{\partial_\omega^2 \sigma'}{\sigma'} \right]_{\omega=0} \sim \left( \frac{\pi T}{\tilde{\gamma}} \right)^2, \quad (17)$$

and we have defined  $\tilde{\gamma}$  as a measure of the ‘‘width’’ of the conductivity, and the expansion is reasonable so long as  $\tilde{\gamma} \gg \pi T$ .

## B. Sharply peaked $\sigma$

If  $\sigma'(\omega)$  is negligible except for frequencies  $|\omega| \ll T$ , the corresponding imaginary time correlator is nearly constant in  $\tau$ , with polynomial corrections given by moments of  $\sigma'(\omega)$ . This can be seen by Taylor expanding the integration kernel for  $|\omega\beta|, |\omega\tau| \ll 1$ :

$$\tilde{\Lambda}(\tau) = \frac{NT}{\pi} \left( 1 - \frac{\gamma^2}{24T^2} + \frac{\gamma^2}{2} [\tau - \beta/2]^2 + \dots \right), \quad (18)$$

where the total optical weight is  $N \equiv \int \sigma'(\omega) d\omega$ , and the squared width of the peak is  $\gamma^2 = N^{-1} \int \omega^2 \sigma'(\omega) d\omega$

## C. Marginal Fermi liquid

The Raman response of many strongly correlated electron fluids can be well approximated (below a high frequency cut-off) by the ‘‘marginal Fermi liquid’’ form

$$\chi''_{\text{MFL}}(\omega) = A \tanh(\beta\omega/2). \quad (19)$$

This same form arises as the local susceptibility of a two-channel Kondo impurity and in various other contexts. Transforming this expression to imaginary time yields

$$\Lambda(\tau) = \frac{AT}{\cos[\pi T(\beta/2 - \tau)]} \quad (20)$$

where the divergences as  $\tau \rightarrow 0$  and  $\tau \rightarrow \beta$  are cut off at short imaginary times of order the inverse cut-off.

## D. Quantum-Critical Power Law

Near a QCP obeying  $\omega/T$  scaling, one expects order parameter correlations to have a power law form for long imaginary times:

$$\tilde{\Lambda}(\tau) \approx A \left[ \frac{1}{|\tau|^x} + \frac{1}{|\beta - \tau|^x} \right]. \quad (21)$$

(The divergences at  $\tau = 0, \beta$  would be regularized at an appropriate UV cutoff scale.) Working backwards, we see that for  $x < 2$ , the corresponding expression in real-time is

$$\chi''(\omega) = \frac{A}{T^{1-x}} F(\beta\omega), \quad (22)$$

where  $F$  is the scaling function

$$F(u) = \frac{\pi u}{\Gamma(x)} \left| \frac{1}{u} \right|^{2-x} \left[ 1 - e^{-|u|} \right]. \quad (23)$$

While this expression in Eqs. 22 and 23 is convenient, as it exactly reproduces the power-law behavior in Eq. 21, as a practical matter we know that the only important aspect is the behavior for  $\omega \sim T$ . Specifically, if  $\gamma$  is a low frequency scale which vanishes at the QCP, and if  $\Omega$  is an ultraviolet cutoff, then the essential aspects of this analysis can be restated as

$$\chi''(\omega) \sim \left[ \frac{\omega}{|\omega|^{2-x}} \right] \begin{cases} \beta|\omega| & \text{for } \gamma \ll |\omega| \ll T \\ 1 & \text{for } T \ll |\omega| \ll \Omega \end{cases} \quad (24)$$

In particular, the relevant critical exponent,  $x$ , can be determined from the power-law behavior in the range  $T \ll \omega \ll \Omega$ , if such exists in experiment.

## VI. RAW DATA OF $\text{Ba}(\text{Fe}_{1-x}\text{Co}_x)_2\text{As}_2$

In Fig. 2 we show the Raman response of overdoped  $\text{Ba}(\text{Fe}_{0.915}\text{Co}_{0.085})_2\text{As}_2$  in  $A_{1g} + A_{2g}$  ( $RR$  polarization) and  $B_{2g} + A_{2g}$  ( $xy$ ) symmetry where the contribution in  $A_{2g}$  symmetry was shown to be negligibly small below  $1000 \text{ cm}^{-1}$ .<sup>11</sup> The insets show the light polarizations with respect to the FeAs plane. Similar  $B_{2g} + A_{2g}$  data were presented by Gallais and coworkers<sup>12</sup>. The spectra become nearly constant and temperature independent to within  $\pm 5\%$  at energies above  $700 \text{ cm}^{-1}$ . Below  $700 \text{ cm}^{-1}$  the intensity increases upon cooling with the  $B_{2g}$  spectra displaying a slightly stronger variation. The temperature dependences of both symmetries are essentially compatible with the variation of the conductivity. Below the superconducting transition temperature  $T_c = 20.5 \text{ K}$  the pair-breaking effect can be observed in the range below  $150 \text{ cm}^{-1}$ . The pair-breaking peaks are marked by arrows.

\* Present address: TNG Technology Consulting GmbH, Beta-Strasse, 85774 Unterf6hring, Germany

<sup>1</sup> M. Randeria, N. Trivedi, A. Moreo, and R. T. Scalettar, Phys. Rev. Lett. **69**, 2001 (1992).

<sup>2</sup> N. Trivedi and M. Randeria, Phys. Rev. Lett. **75**, 312 (1995).

<sup>3</sup> N. Trivedi, R. T. Scalettar, and M. Randeria, Phys. Rev. B **54**, R3756 (1996).

<sup>4</sup> We use the crystallographic two-iron unit cell. In the one-iron unit cell this would be  $B_{1g}$ .

<sup>5</sup> B. S. Shastry and B. I. Shraiman, Phys. Rev. Lett. **65**, 1068 (1990).

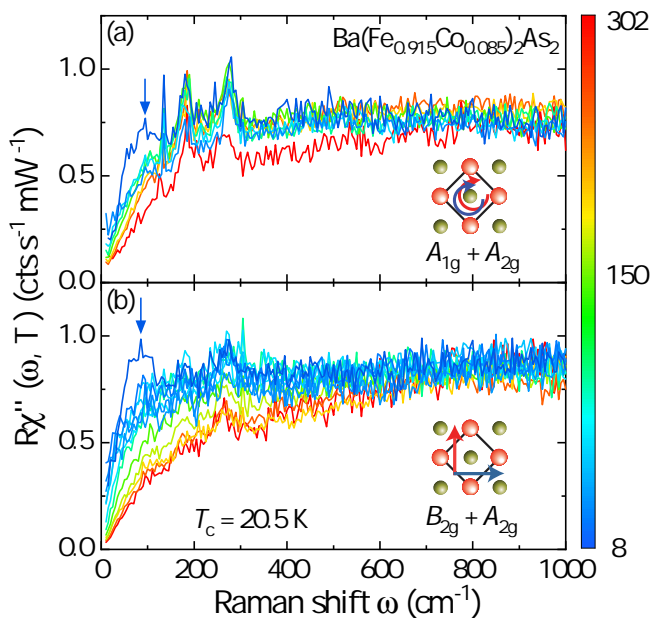


FIG. 2: Raw data of the Raman response  $R\chi''(\Omega, T)$  of  $\text{Ba}(\text{Fe}_{0.915}\text{Co}_{0.085})_2\text{As}_2$ . We use a continuous color scale for the temperature (right scale bar). The (a)  $A_{1g} + A_{2g}$  and (b)  $B_{2g} + A_{2g}$  spectra are measured in  $RR$  ( $R = 1/\sqrt{2}(x+iy)$ ) and  $xy$  polarization, respectively, where  $x$  and  $y$  are the axes of the 2 Fe crystallographic cell in the tetragonal phase. Arrows indicate the pair-breaking peaks.

- <sup>6</sup> C. Varma, P. B. Littlewood, S. Schmitt-Rink, E. Abrahams, and A. Ruckenstein, *Physical Review Letters* **63**, 1996 (1989).
- <sup>7</sup> F. Kretschmar, T. Böhm, U. Karahasanović, B. Muschler, A. Baum, D. Jost, J. Schmalian, S. Caprara, M. Grilli, C. Di Castro, et al., *Nature Phys.* **12**, 560 (2016).
- <sup>8</sup> Y. Gallais and I. Paul, *Comptes Rendus Physique* **17**, 113 (2016).
- <sup>9</sup> Y. Schattner, S. Lederer, S. A. Kivelson, and E. Berg, *Physical Review X* **6**, 031028 (2016).
- <sup>10</sup> S. Lederer, Y. Schattner, E. Berg, and S. A. Kivelson, *Proceedings of the National Academy of Sciences* **114**, 4905 (2017), .
- <sup>11</sup> B. Muschler, W. Prestel, R. Hackl, T. P. Devereaux, J. G. Analytis, J.-H. Chu, and I. R. Fisher, *Phys. Rev. B* **80**, 180510 (2009).
- <sup>12</sup> Y. Gallais, R. M. Fernandes, I. Paul, L. Chauvière, Y.-X. Yang, M.-A. Méasson, M. Cazayous, A. Sacuto, D. Colson, and A. Forget, *Phys. Rev. Lett.* **111**, 267001 (2013)